Estimating Plume Volume for Geologic Storage of CO_2 in Saline Aquifers

Christine Doughty
Earth Sciences Division
Lawrence Berkeley National Laboratory

July 2008

Typically, when a new subsurface flow and transport problem is first being considered, very simple models with a minimal number of parameters are used to get a rough idea of how the system will evolve. For a hydrogeologist considering the spreading of a contaminant plume in an aquifer, the aquifer thickness, porosity, and permeability might be enough to get started. If the plume is buoyant, aquifer dip comes into play. If regional groundwater flow is significant or there are nearby wells pumping, these features need to be included. Generally, the required parameters tend to be known from pre-existing studies, are parameters that people working in the field are familiar with, and represent features that are easy to explain to potential funding agencies, regulators, stakeholders, and the public.

The situation for geologic storage of carbon dioxide (CO_2) in saline aquifers is quite different. It is certainly desirable to do preliminary modeling in advance of any field work since geologic storage of CO_2 is a novel concept that few people have much experience with or intuition about. But the parameters that control CO_2 plume behavior are a little more daunting to assemble and explain than those for a groundwater flow problem. Even the most basic question of how much volume a given mass of injected CO_2 will occupy in the subsurface is non-trivial. However, with a number of simplifying assumptions, some preliminary estimates can be made, as described below.

To make efficient use of the subsurface storage volume available, CO_2 density should be large, which means choosing a storage formation at depths below about 800 m, where pressure and temperature conditions are above the critical point of CO_2 (P = 73.8 bars, T = 31^{o}C). Then CO_2 will exist primarily as a free-phase supercritical fluid, while some CO_2 will dissolve into the aqueous phase.

A mass balance for CO_2 may be written as

$$M = < \phi S_g \rho_g > V + < \phi S_l X_l \rho_l > V \qquad (1)$$

where M is the total mass of CO_2 injected, ϕ is the porosity of the storage formation, S_g is the saturation of free-phase CO_2 (that is, the fraction of pore space filled with free-phase CO_2), $S_l = 1 - S_g$ is the saturation of the aqueous phase (water plus dissolved salt plus dissolved CO_2), ρ_g and ρ_l are densities of the CO_2 and aqueous phases, respectively, X_l is the mass fraction of CO_2 dissolved in the aqueous phase, and V is plume volume. Angle brackets represent a spatial average over the plume. The first term of Equation (1) represents the mass of free-phase CO_2 and the second term the mass of dissolved CO_2. Assuming that ϕ, S, ρ, and X_l are not correlated enables the angle brackets to be dropped,

with the understanding that each variable represents the average value over the plume. Solving for V yields

$$V = \frac{M}{\phi(S_g \rho_g + (1 - S_g) X_l \rho_l)} \qquad (2)$$

To determine V, first we need a value for ϕ, the average porosity of the storage formation, which is typically known, at least approximately, based on the geological setting.

Next, we need ρ_g, the density of the free-phase CO_2, at the pressure and temperature conditions of the storage formation. Often (P, T) information is unknown for candidate sites, but assuming a hydrostatic pressure gradient and a geothermal temperature gradient provide a good first guess. In the absence of any site-specific information, $P = 1+0.1z$, with P in bars and depth z in meters, and $T = 15 + 0.025z$, which gives T in degrees C, may be used. Armed with (P,T) conditions, a standard CO_2 equation-of-state package (for example, http://lnx.lbl.gov/gaseos/gaseos.html) provides the density of free-phase CO_2, ρ_g, as illustrated in Figure 1. Values of ρ_g for a range of conditions considered reasonable for geologic storage are shown in Table 1.

Next, we need X_l, the mass fraction of dissolved CO_2 in the aqueous-phase fluid. We approximate X_l as the solubility of CO_2 in brine. That is, we assume that all dissolved CO_2 is in equilibrium with free-phase CO_2. With this assumption, X_l depends only on pressure, temperature, and brine salinity, as illustrated in Table 1.

Next, we need ρ_l, the density of the aqueous phase, at the pressure, temperature, and salinity conditions of the storage formation. The aqueous-phase density ρ_l depends weakly on P, T, and X_l and varies more strongly with brine salinity, as illustrated in Table 1.

Finally, we need an estimate for CO_2 saturation, S_g. Recall that when CO_2 is injected into a saline aquifer, the brine is not simply pushed away from the well and replaced with CO_2. A two-phase flow region develops, with CO_2 bypassing some of the brine. The pore-scale details of interaction between the CO_2 phase and the aqueous phase are generally represented at the macro-scale by what are known as characteristic curves: capillary pressure and relative permeability as functions of phase saturation. The parameters and functional forms of the characteristic curves, along with the viscosity ratio of the CO_2 and brine, determine S_g within the CO_2 plume. Basic arguments about molecular structure indicate that for saline aquifers, supercritical CO_2 is the non-wetting phase and brine is the wetting phase. Thus CO_2 is analogous to oil in oil/water two-phase systems, enabling us to tap into the extensive petroleum literature for information on characteristic curves. Two key parameters of the characteristic curves are the residual phase saturations: the saturations below which a phase is immobile. In practical terms, residual liquid saturation S_{lr} determines how much water is bypassed as CO_2 invades the pore space, and residual gas saturation S_{gr} determines how much CO_2 is trapped when water imbibes back into the pore space (Doughty et al., 2007). The value of S_g to use in Equation (2) can best be determined by numerical simulation, but theoretically it should fall between S_{gr} and (1

– S_{lr}). However, it is unlikely that these parameters will be known at the early stage of an investigation. To make matters worse, there is no single value of S_{gr} that can be specified for the CO_2 plume as a whole – S_{gr} depends on the saturation history of each location within the plume. For moderate to high permeability saline aquifers that are typical CO_2 storage targets, literature values of S_{lr} are generally less than 0.3 and S_{gr} is generally less than 0.4. Thus, it is reasonable to expect S_g to be in the range 0.4–0.7. A good first guess is $S_g = 0.5$.

Substituting estimated values of ϕ, S_g, ρ_g, ρ_l, and X_l into Equation (2) provides an estimate of V, the volume that a mass M of injected CO_2 occupies in the subsurface. Moreover, because S_g and S_l are comparable, ρ_g and ρ_l differ by less than a factor of two, and X_l is just a few percent, we find that the fraction of CO_2 in the supercritical phase is much larger than the fraction that is dissolved.

The next natural question is when are these estimates of V and phase partitioning applicable? For early-stage investigations, we are likely most interested in the time period during and shortly after CO_2 injection. For this time frame, we can safely neglect slow processes such as mineral reactions (Xu et al., 2004) and aqueous-phase convection (Ennis-King and Paterson, 2005). Then the only parameter in Equation (2) likely to change significantly as the CO_2 plume evolves is S_g.

The variation of S_g is intimately connected with the functional form of the characteristic curves (Doughty, 2007). In the petroleum industry, it is well accepted that characteristic curves are hysteretic. That is, the drainage process (non-wetting-phase CO_2 replacing wetting-phase brine) is not simply reversed in the imbibition process (wetting-phase brine replacing non-wetting-phase CO_2). The key parameter of the characteristic curves for trapping CO_2, the residual gas saturation S_{gr}, is considered to be zero during drainage, and to be non-zero and history-dependent during imbibition (Land, 1968).

As shown in the top frame of Figure 2, while CO_2 injection is occurring, the CO_2 plume is growing everywhere, so drainage is the dominant process and $S_{gr} = 0$. To calculate V at the end of the CO_2 injection period, the Buckley-Leverett (1942) analytical solution for a radial-geometry plume may be used to approximate S_g. For viscosity ratios in the range shown in Table 1, the simple relation $S_g = 0.5(1 - S_{lr})$ provides a reasonable fit to the Buckley-Leverett solution employing the commonly-used Corey (1954) relative permeability functions.

Once injection ceases, and the plume moves upward and updip due to buoyancy forces, different locations experience drainage and imbibition at different times, as illustrated in the bottom frame of Figure 2. At the leading edge of the plume, drainage continues with $S_{gr} = 0$. At the trailing edge, imbibition occurs with $S_{gr} > 0$. Thus the plume is more mobile at the leading edge than at the trailing edge, so it stretches out as it moves, which lowers S_g. When saturation everywhere drops to S_{gr}, the entire plume becomes immobilized, a phenomenon known as capillary trapping. To estimate V at this time, the maximum value of S_{gr}, a material property denoted S_{grmax}, provides an upper limit for S_g. The petroleum literature (Holtz, 2005) suggests that S_{grmax} decreases as porosity increases,

and typically ranges between 0.2 and 0.4 for moderate to high permeability saline aquifers.

Note from Equation (1) that as S_g decreases, the fraction of injected CO_2 that is dissolved increases. This leads to an interesting trade-off between capillary trapping and dissolution. For smaller values of S_{grmax}, capillary trapping is less effective in that the plume moves farther and spreads more before becoming immobilized, but this exposes the CO_2 plume to more native brine, enabling more dissolution (Doughty and Myer, 2008).

The simple methodology described here for estimating plume volume can provide a useful starting point for subsequent numerical modeling, which is necessary to capture the complex interplay between phase interactions, buoyancy flow, and geologic heterogeneity that occurs as CO_2 is injected into a saline aquifer.

Acknowledgments

This work was supported by the Assistant Secretary for Fossil Energy, Office of Coal and Power Systems, through the National Energy Technology Laboratory under U.S. Department of Energy Contract No. DE-AC02-05CH11231.

References

Buckley, S.E. and Leverett, M.C. 1942. Mechanism of fluid displacement in sands. *Trans. Am. Inst. Min. Metall. Eng.* 146, 107-116.

Corey, A.T. 1954. The interrelation between gas and oil relative permeabilities. *Producers Monthly* November, 38-41.

Doughty, C. 2007. Modeling geologic storage of carbon dioxide: comparison of non-hysteretic and hysteretic characteristic curves. *Energy Conversion and Management* 48(6), 1768-1781, doi:10.1016/j.enconman.2007.01.022.

Doughty, C., Freifeld, B.M., Trautz, R.C. 2007. Site characterization for CO_2 geologic storage and vice versa – The Frio brine pilot, Texas, USA as a case study. *Environmental Geology*, doi:10.1007/S00254-007-0942-0.

Doughty, C. and Myer, L.R. 2008. Scoping calculations on leakage of CO2 in geologic storage. In: McPherson, B. and Sundquist, E., editors, *Science and technology of carbon sequestration*, American Geophysical Union, Washington DC, in press.

Ennis-King, J. and Paterson, L. 2005. Role of convective mixing in the long-term storage of carbon dioxide in deep saline formations (SPE 84344). *SPE Journal* 10(3), 349-356.

Holtz, M.H. 2005. Reservoir characterization applying residual gas saturation modeling, example from the Starfak T1 reservoir, middle Miocene Gulf of Mexico, M.Sc. Thesis, University of Texas at Austin

Land, C.S. 1968. Calculation of imbibition relative permeability for two- and three-phase flow from rock properties (SPE 1942). *SPE Journal* June, 149-56.

Pruess, K., Oldenburg, C., Moridis, G. 1999. TOUGH2 user's guide, version 2.0. *Rep. LBNL-43134*. Lawrence Berkeley National Laboratory, Berkeley, CA.

Pruess, K. 2005. ECO2N: A TOUGH2 Fluid Property Module for Mixtures of Water, NaCl, and CO_2. *Rep. LBNL-57952*. Lawrence Berkeley National Laboratory, Berkeley, CA.

Spycher, N. and Pruess. K. 2005. CO_2-H_2O Mixtures in the Geologic Sequestration of CO_2. II. Partitioning in Chloride Brines at 12–100 ˚C and up to 600 bar. *Geochim. Cosmochim. Acta* 69(13), 3309–3320, doi:10.1016/j.gca.2005.01.015.

Xu, T., Apps, J.A., and Pruess, K. 2004. Numerical simulation of CO_2 disposal by mineral trapping in deep aquifers. *Applied Geochemistry* 19, 917-936.

Table 1. Properties of free-phase CO_2 and CO_2-saturated brine for a range of conditions considered reasonable for geologic storage of CO_2 in saline aquifers. Pressure P (bars) and temperature T (^oC) determined using hydrostatic and geothermal gradients, respectively. Density ρ (kg/m^3), viscosity μ ($Pa \cdot sec$), and dissolved CO_2 mass fraction X_l. calculated with the TOUGH2 numerical simulator (Pruess et al., 1999) using the ECO2N equation of state package (Pruess, 2005; Spycher and Pruess, 2005).

Depth	CO_2		0 mg/L Brine			50,000 mg/L Brine			100,000 mg/L Brine		
(m)	ρ_g	μ_g	ρ_l	μ_l	X_l	ρ_l	μ_l	X_l	ρ_l	μ_l	X_l
z=1000 P=101 T=40	635	0.49E-4	1007	0.65E-3	0.052	1037	0.72E-3	0.042	1069	0.80E-3	0.033
z=1500 P=151 T=52.5	681	0.55E-4	1004	0.53E-3	0.052	1034	0.58E-3	0.041	1067	0.65E-3	0.033
z=2000 P=201 T=65	694	0.57E-4	1000	0.44E-3	0.052	1030	0.48E-3	0.041	1063	0.54E-3	0.033
z=2500 P=251 T=77.5	701	0.58E-4	995	0.37E-3	0.053	1025	0.41E-3	0.042	1058	0.46E-3	0.034

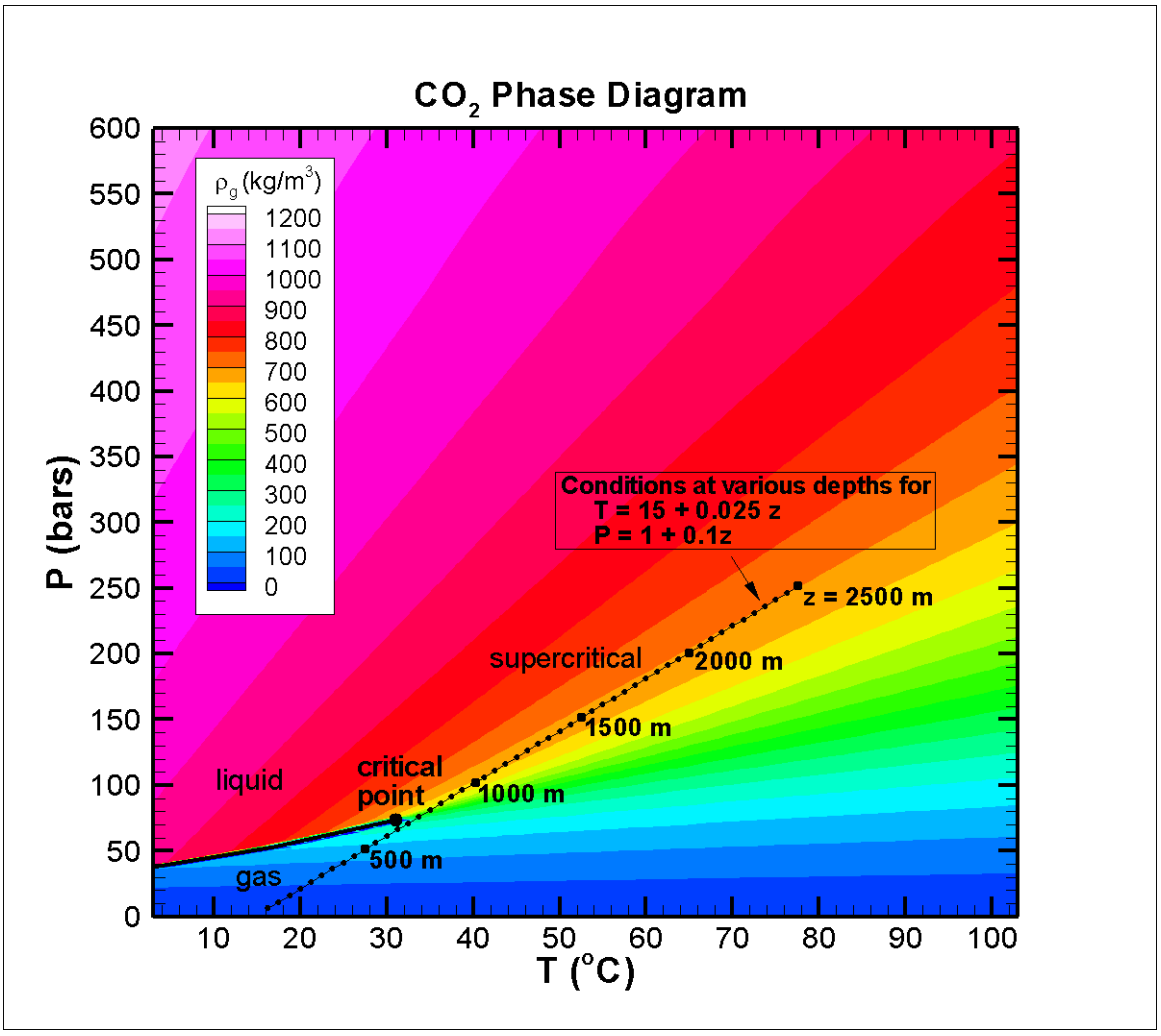

Figure 1. Density of CO_2 as a function of pressure *P* and temperature *T*. The black line shows the saturation line, which separates liquid and gaseous phases. Beyond the critical point, CO_2 exists as a supercritical phase. Assuming functional forms for the dependence of *P* and *T* on depth enables CO_2 density at various depths to be estimated, as shown by the dashed line.

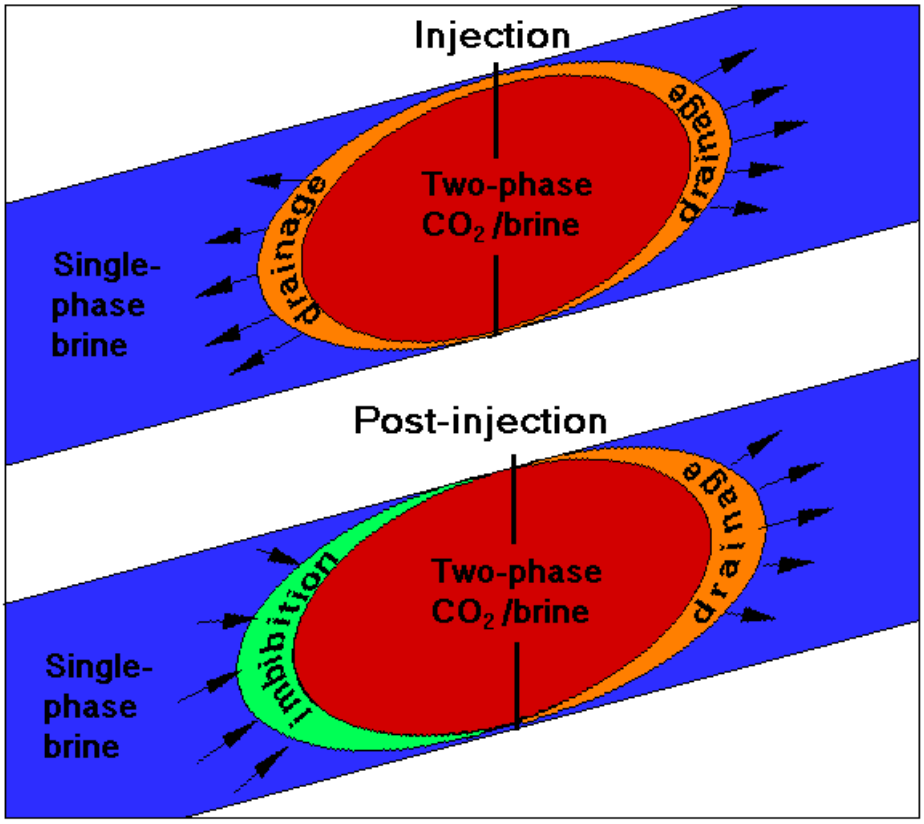

Figure 2. Schematic of CO_2 injection period (top), in which drainage occurs at all plume boundaries (orange), and post-injection period (bottom), in which drainage occurs at the leading edge of the plume on the right (orange) and imbibition occurs at the trailing edge of the plume on the left (green) as the plume migrates, e.g. by buoyancy forces.